A. Visagan ✉
P. Ganesh
N. Ethiraj
K. Kalaichelvan

https://doi.org/10.21278/TOF.482054923
ISSN 1333-1124
eISSN 1849-1391

MULTI-OBJECTIVE OPTIMIZATION OF SINGLE POINT INCREMENTAL FORMING OF 316L STAINLESS STEEL USING GREY RELATIONAL AND PRINCIPAL COMPONENT ANALYSES

Summary

The single point incremental forming process has a wide range of applications, and the process can be carried out without any specialized tooling and punches. However, if the process parameters are not carefully chosen, the components being manufactured are limited. This paper presents the single point incremental forming of 316L stainless steel sheets of 0.8 mm in thickness by varying input process parameters, such as tool diameter, wall angle, step depth, spindle speed, and feed rate, to study their effect on output parameters, strain and surface roughness. The Taguchi method was coupled with principal component analysis to identify the optimum process parameter combination to improve strain and reduce surface roughness. The wall angle has been determined to be the most influential process parameter, and the analysis of variance showed that the wall angle had the highest contribution (52.44 %), followed by step depth (18.55 %), tool diameter (9.72 %), spindle speed (1.64 %), and feed rate (0.83 %). The suggested design of experiments determined the best process parameter combination and executed the confirmation run. The grey relational analysis combined with principal component analysis improved the single point incremental forming of 316L stainless steel sheets.

Key words: *Single Point Incremental Forming, 316L Stainless Steel, Optimization, Grey Relation Analysis, Principal Component Analysis, ANOVA*

1. Introduction

Single Point Incremental Forming (SPIF) is a widely used alternative process in the sheet metal industry; it is used for producing symmetric and asymmetric structures using Computer Numerical Control (CNC) machines. The SPIF process was performed with a cylindrical tool with a hemispherical or a flat head to follow the CNC tool path in the CNC machine. The SPIF process parameters such as tool diameter and profile are used to create prototypes, panels, and coverings for biomedical applications.

Experiments were conducted to predict the minimal time for producing 1.2 mm-thick 1060-O aluminium alloy sheets [1]. The Taguchi analysis indicated vertical pitch as the most essential metric. The tool diameter, vertical pitch, and feed interacted strongly during the

forming process. In the forming of 2024-O aluminium alloy sheets, Hussain et al. [2] observed no significant influence of the sheet thickness or tool size separately but a substantial interaction between the two. The experiments indicated that smaller tool sizes could not create thick sheets.

Salah Echrif and Maftah Hrairi [3] performed incremental shaping on 0.1mm-thick 1050-O aluminium alloy sheets. They varied the Taguchi parameters to study surface roughness. The increased tool radius with a shallower increment depth provided lower surface roughness. The grey relational analysis (GRA) and response surface methodology (RSM) identified optimal responses on a 0.4 mm-thick stacked copper sheet. The experiment feed rate was shown to be the most important factor affecting springback and surface roughness. The plots revealed a strong connection between the stacking of sheets and the vertical step down. The grey relational grade (GRG) produced suggests that the proposed optimization strategy may be used for metal forging [4].

Taleb Araghi et al. [5] proposed a hybrid approach to the forming of the titanium alloy, TiAl6V4, and the magnesium alloy, Mg-AZ31B; due to the hybrid approach, the forming time was reduced and the component precision improved. Laser heating improves the formability of titanium and magnesium alloys.

Amrut Mulay et al. [6] used the Design of Experiments (DOE) to increase the surface quality and formability of the 1050-O aluminium alloy. The findings show that sheet thickness and step depth influence surface quality and formability. The tool with a diameter of 8 mm produced negligible springback effects compared to those produced by the tools with diameters of10 mm and 12 mm, respectively. A larger tool diameter reduces the maximum forming angle. Lu et al. [7] used the grey relational and principal component analyses to enhance the milling of SKD61 tool steel. The proposed optimization method simplifies the correlated variables while preserving the original data. The results confirm that the approach proposed in this study can be a useful tool to improve the cutting performance of rough cutting processes in high-speed end milling processes.

Pandivelan Chinnayan and Jeevanantham [8] used single-point incremental forming to manufacture cold-rolled 5052 aluminium alloy sheets. The grey relational analysis was used to improve surface roughness and strain sum. The weighting values were obtained using the principal component analysis. The ball-end tool and lubrication minimized friction on the sheet being produced. Surface roughness reduces formability. Vishal Gulati et al. [9] used three different values of sheet thickness, two different tool radii, and three different lubricants to create the 6063 aluminium alloy. The Taguchi analysis was carried out for the optimization of process parameters to get better results. The surface roughness and component angle were measured for all the components formed. Among the output parameters, the grey relational coefficient (GRC) was found to be the most outstanding process parameter influencing surface roughness. The forming wall angle increases with sheet thickness and tool rotational speed.

Pratheesh Kumar and Elangovan [10] used the response surface methodology to form Inconel 718, utilizing incremental forming to improve the roughness, profile accuracy, and thickness of the formed component. Surface roughness increases with step depth. Similarly, viscosity increases surface roughness. Reducing the feed rate and vertical step depth may aid in the control of springback. Following single-point incremental forming, Suresh Kurra et al. [11] used finite element analysis (FEA) to find responses for Extra Deep Drawing (EDD) steel sheet forming force, permanent strain, and thinning. The Taguchi orthogonal array was used in FEA simulations. Numerical simulations were done in Python and MATLAB, customized for SPIF.

Ajay Kumar and Vishal Gulati implemented the Taguchi analysis [12] and carried out experiments on the incremental forming of 2024-O and 6063-O aluminium alloy sheets. The forming force was determined using flat and hemispherical tools of varied sizes. Axial force decreased as the wall angle increased up to 68 degrees, resulting in failure. A hemispherical

tool produced the weakest forming force, whereas a flat-ended tool produced the strongest. Ajay Kumar and Vishal Gulati [13] optimized the forming of 2024-O and 6063-O aluminium alloy sheets by employing flat and hemispherical tool forms. A flat-end tool produced inadequate surface roughness, whereas a hemispherical tool produced exceptionally good surface roughness. Angshuman Baruah et al. [14] managed to produce good-quality 5052-H32 aluminium sheets using the SPIF technique. Feed rate had the weakest influence on optimum formability and surface polish, whereas lubrication had the strongest.

Mariem Dakhli et al. [15] used GRA to optimize forming forces, forming time, and surface roughness in the forming of 1050 aluminium alloy steel, DC01 non-alloy cold-rolled steel, and CuB2 copper alloy steel. The interaction between the rotating tool speed and feed rate was found to be strong. Seyed Ali Asghar Asghari et al. [16] used GRA in single-point and two-point incremental forming processes performed on 1050 aluminium alloy sheets. The results confirmed that the high spindle speed affects formability by causing sheet thinning due to the friction created.

Hani Mostafanezhad [17] optimized the maximum resultant force and thinning ratio in the two-point incremental forming of 1050 aluminium. The wall angle was found to be an essential factor influencing the thinning ratio, and sheet thickness was the one influencing the forming force Maji and Gautam Kumar [18] calculated the forming wall angle, sheet thickness, and surface quality of 5083 AA sheets. The proposed algorithm proved to be accurate in obtaining good output responses.

Visagan A. et al. [19] performed SPIF experiments on an AISI 316 L sheet of uniform thickness. The forming parameters, such as wall angle, feed rate, tool rotational speed, and depth of forming, were varied. The difference between the test results and measured values for a wall angle of 67º is between 1.49% and 4.48%. When the wall angle was 65º, the spindle speed was 200 rpm, the feed rate was 1000 mm/min, the step depth was 0.2 mm, and the surface roughness was 0.57 μm. For lower values of step depth and feed rate, the forming time was maximum and vice versa. A minimum wall thickness of 0.12 mm was observed near the bottom wall angle. Ganesh P et al. [20] conducted experiments in the single-point incremental forming of 5052 aluminim alloy sheets to find the most optimum process parameter for obtaining minimum surface roughness and maximum wall angle. The adopted optimization method achieved good results for a feed rate of 500 mm/min, step depth of 0.4 mm, tool diameter of 10 mm, and spindle speed of 300 rpm. Among the considered input forming parameters, the diameter of the tool used in the process had the greatest influence on surface roughness, and tool rotational speed had the highest impact on wall angle.

Visagan A et al. [21] conduted Two-Point Incremental Forming (TPIF) on AISI 316L sheets of uniform thickness for a double-wall angle cone. The Taguchi grey relational analysis and the Technique for Order Preference by Similarity to Ideal Solution (TOPSIS) were employed, and the optimization results of both methods were compared. The tool rotational speed and step of forming were the most influential process parameters obtained from GRA and TOPSIS, respectively. An improvement in the grey relational grade (GRG) of 0.3145 was obtained from the method proposed by GRA, and an improvement in the closeness coefficient of 0.1324 was obtained from TOPSIS. Visagan A et al. [22] conducted two-point incremental forming on AISI 316 L sheets, keeping a single wall angle cone as the target geometry. The wall angle of the component was fixed at 66º, whereas the other parameters, such as tool diameter, step depth, spindle speed, and feed rate, were varied at three different levels. The experiment results revealed that as the step depth increased, the height of forming also increased; on the other hand, a greater step depth may also produce an over-formed component. A wall angle of 65.12º was obtained when the step depth was kept at the maximum level; that value is the closest value to that of the target geometry. Aminimum forming time of 65 minutes

was obtained when the step depth was kept at the maximum level. When the roughness of the components was measured in all trials, it was observed that the component roughness was at its minimum in the centre and at its maximum at the top.

Hongwei Gao et al. [23] performed a dynamic simulation of cross-wedge rolling of LZ50 axle steel. The work was carried out to study the stress, strain, and temperature fields of the workpiece in the forming process. The workpiece experienced radial compression, axial extension, and lateral deformation when a wedge-shaped die was used. The influence of lateral deformation on the deformation of the workpiece was minimal. In the stress field analysis, compressive stress was noted at the wedging section while tensile and compressive stresses were both identified at the widening and finishing sections. In the temperature analysis, the uniform temperature was recorded on the surface and the internal areas.

Loganathan et al. [24] used the Taguchi design of experiments to optimize the single point incremental forming of 6061 aluminium alloy sheets with a thickness of 1.15 mm. A step depth of 0.5 mm, tool rotational speed of 200 rpm, and feed rate of 400 mm/min were identified as the optimum combination of process parameters for obtaining a good surface finish and better wall thickness. The step depth made a maximum contribution of 28.09%, followed by a tool rotational speed contribution of 24.40 %, and that of the feed rate of 21.94%. The proposed method was fairly accurate; the accuracy of the method can be further improved by applying relevant multi-criteria decision-making algorithms in future experiments.

Karthick et al. [25] studied the variation in tensile properties of AISI 304 stainless steel during gas metal arc welding. The gas metal arc variants were used under optimised conditions, and a single V-butt groove with an angle of 60^{o} and a thickness of 12 mm was produced. The cold metal transfer gave an effective tensile strength of 657 MPa. The maximum elongation observed was 19%, while that of the base metal was 45%. The results proved that due to the electromagnetic force exerted during the cold metal transfer process, the tensile strength value was the highest compared to those in the other proposed methods. The cold metal transfer joint received a minimal heat input, resulting in a good joint efficiency and notch strength ratio.

Zhongfeng Zhang et al. [26] investigated the influence of paths on the outcomes of the multi-point forming of double-curved pieces made of 1561 aluminium alloy by adopting a multi-stage forming technique. The ABAQUS finite element simulation software was used to do the numerical modelling of the multi-step shaping of curved sheets. The simulation findings show that the shaping of 1561 aluminium alloy double-curved components is characterized by wrinkling and low forming accuracy in single-step forming, but the accuracy and forming quality improve greatly after four-step forming. As a result, a four-step forming approach was used for stamping testing on double-curved components. The findings of the GOM-inspect accuracy inspection of formed components show that a four-step process may successfully enhance the quality of curved parts.

Wafa Taktak et al. [27] performed an experimental investigation into the fracture toughness of the AA5754 H111 aluminium alloy under cold rolling reduction. A ductile tearing test was conducted to determine the fracture toughness of the workpiece before and after cold rolling. The mechanical characteristics of the unrolled and rolled AA5754 H111 aluminium alloys were investigated using standard tensile tests in two directions as well as microhardness testing. The cold rolling had a substantial influence on the fracture toughness parameter and the mechanical characteristics of the AA5754 H111 aluminium alloy in the rolling and transversal directions, according to the findings. The maximum strength was found in the radial direction, whereas the greatest ductility was discovered in the transversal direction.

In this study, single wall angle cones were formed by varying input process parameters such as tool diameter, wall angle, step depth, spindle speed, and feed rate. The output responses, namely strain 1 (parallel to rolling direction), strain 2 (perpendicular to rolling direction), strain

3 (diagonal to rolling direction), and the surface roughness parameters Ra1, Ra2, and Ra3, were studied and measured in the same direction as the strain was measured. The optimization was carried out using the grey relational analysis (GRA) coupled with the principal component analysis (PCA); the optimal combination to get improved strain was identified, and the minimum surface roughness was calculated. The SEM analysis was carried out for the optimal parameter combination.

2. Materials and Methodology

A circular cone was chosen as the geometric profile for the single-point incremental forming of 0.8 mm thick 316L stainless steel sheets. Figure 1 (a) shows the SPIF process, while Figure 1 (b) shows the target geometry created in the Pro-E design software. The SPIF experiments were planned using a Vertimach V-510 Tal CNC milling machine, Figure 2. The workpiece prepared for forming was a square sheet measuring 250 x 250 mm with a uniform thickness of 0.8 mm. One side of the sheet was laser-etched with 4 mm circles and 1 mm gaps between them to determine the surface strain during the SPIF process. The workpieces were formed using 8 mm and 10 mm carbide tools with hemispherical tips.

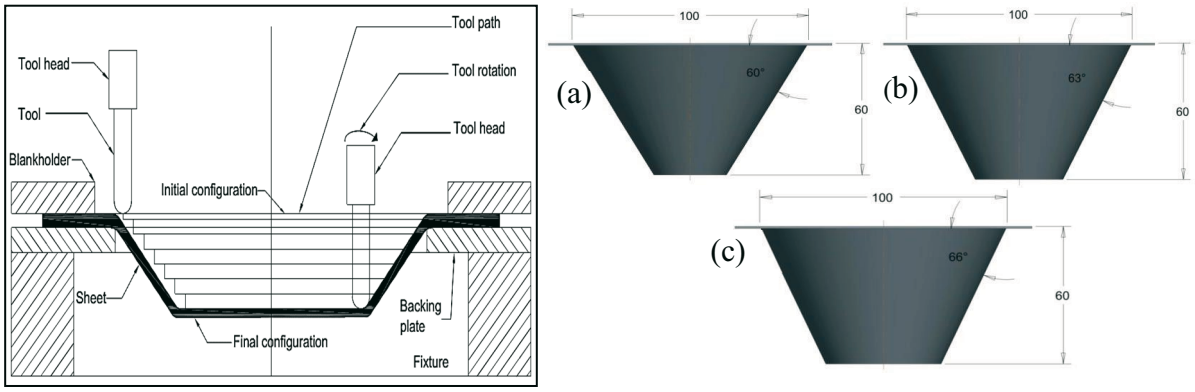

Fig. 1 **(a)** Schematic representation of the SPIF process; **(b)** Dimensions of the target geometry

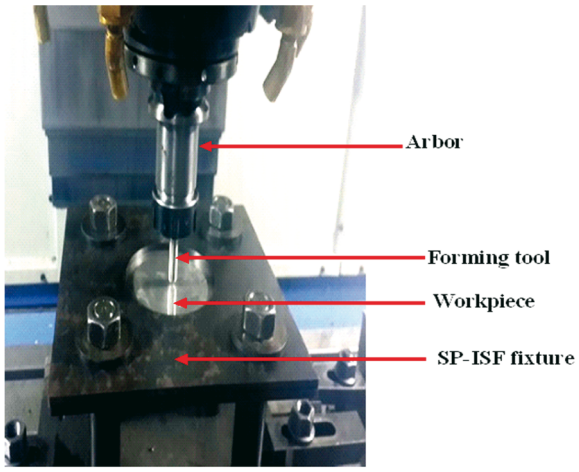

Fig. 2 CNC milling machine used for the experiments

Taguchi's experimentation is used to anticipate optimal parameter selections in this study. The degree of freedom must be determined to pick the best design. The Degree of Freedom (DOF) is [2-1] + [4 (3-1)] + 1 = 10. Therefore, L_{18} Orthogonal Array (OA) was used, and L_{18} (2^1 x 3^4) was picked. Table 1 shows the factors and levels selected for this investigation, and Table 2 shows the output responses of each experimental combination.

Table 1 Experimental values and their levels

Input Factors		Levels		
		Level 1	Level 2	Level 3
Tool diameter (mm)	A	8	10	
Wall angle (°)	B	60	63	66
Step depth (mm)	C	0.2	0.3	0.4
Spindle speed (rpm)	D	100	200	300
Feed rate (mm/min)	E	500	1000	1500

Table 2 Experimental layout and the response variables using L_{18} orthogonal array (OA)

Exp. no	Forming parameters and their levels					Response variable					
	Tool diameter	Wall angle	Step depth	Spindle speed	Feed rate	Strain 1	Strain 2	Strain 3	Ra 1	Ra 2	Ra 3
1	8	60	0.2	100	500	0.8463	0.1574	0.8643	1.0110	1.3641	1.6931
2	8	60	0.3	200	1000	0.8010	0.1040	0.9234	1.0025	1.2351	1.4996
3	8	60	0.4	300	1500	0.7214	0.2947	0.7656	1.0100	1.3631	1.6916
4	8	63	0.2	100	1000	0.9083	0.1129	0.9995	1.0005	1.1591	1.3856
5	8	63	0.3	200	1500	0.8195	0.1426	0.8599	1.0410	1.3941	1.7381
6	8	63	0.4	300	500	0.8443	0.1011	0.8836	1.2350	1.5881	2.0291
7	8	66	0.2	200	500	0.9706	0.0922	0.9913	1.4530	1.8061	2.3561
8	8	66	0.3	300	1000	0.9388	0.0806	0.9535	1.0049	1.3381	1.6541
9	8	66	0.4	100	1500	0.9589	0.1715	0.9943	1.5820	1.9351	2.5496
10	10	60	0.2	300	1500	0.9877	0.2694	0.9979	1.2291	1.4906	1.0025
11	10	60	0.3	100	500	0.9194	0.2452	0.9216	1.6531	2.1266	1.3000
12	10	60	0.4	200	1000	0.7908	0.3161	0.8851	1.3991	1.7456	1.0460
13	10	63	0.2	200	1500	0.9434	0.1657	0.9725	1.4741	1.8581	1.1210
14	10	63	0.3	300	500	0.8962	0.1592	0.9396	1.6261	2.0861	1.2730
15	10	63	0.4	100	1000	0.9463	0.2091	0.9591	1.8551	2.4296	1.5020
16	10	66	0.2	300	1000	0.9976	0.1027	0.9359	1.3441	1.6631	1.0126
17	10	66	0.3	100	1500	0.9424	0.0937	0.9467	1.2381	1.5041	1.0003
18	10	66	0.4	200	500	0.9156	0.1693	0.9126	1.1541	1.3781	1.0078

3. Results, Analysis, and Discussion

The current study uses the grey relational analysis (GRA) coupled with the principal component analysis (PCA) to optimise strain and surface roughness. The orthogonal array determines the experimental data using the appropriate process parameters. The observed outputs were surface roughness and strain for the circular cone geometry. To achieve maximum strain and minimum surface roughness, a mixed-level L_{18} orthogonal array was developed. The signal-to-noise (S/N) ratio was calculated using Equations (1) and (2) for surface roughness and strain, respectively, and the values are shown in Table 3.

For "the smaller, the better", the S/N ratio (η) = $-10\log_{10}\left(\frac{1}{n}\right)\sum_{i=1}^{n}(y_{ij}^2)$ (1)

For "the larger, the better", the S/N ratio (η) = $-10\log_{10}\left(\frac{1}{n}\right)\sum_{i=1}^{n}(1/y_{ij}^2)$ (2)

Here 'n' stands for replications, and y_{ij} is the response.

The S/N ratio normalization for strain and surface roughness has been determined using Equations (3) and (4), and the calculated values are shown in Table 4. The grey relational coefficient (GRC) and grey relational grade (GRG) are calculated using Equation (5) and Equation (6), respectively.

$$Z_{ij} = \frac{(\max Y_{ij} - Y_{ij})}{(\max Y_{ij} - \min Y_{ij})} \tag{3}$$

$$Z_{ij} = \frac{(Y_{ij} - \min Y_{ij})}{(\max Y_{ij} - \min Y_{ij})} \tag{4}$$

For GRC,

$$\xi_{ij} = \frac{\Delta_{\min} + \lambda\Delta_{\max}}{\Delta_{ij} + \lambda\Delta_{\max}}, \tag{5}$$

where, λ is the distinguishing coefficient, ($0 \leq \lambda \leq 1$). GRG is calculated and shown in Table 6.

$$G_i = \frac{1}{m}\sum_{j=1}^{m} \mu_j \xi_{ij}, \tag{6}$$

where m is the number of responses, and μ_j is the normalised weighting value from PCA shown in Table 6. Principal component analysis is a numerical method for constructing variance-covariance using linear groups of each constraint. The unique multi-objective matrix Y is formed using Equation (7).

$$Y = \begin{bmatrix} y_1(1) & y_1(2) & .... & y_1(n) \\ y_2(1) & y_2(2) & .... & y_1(n) \\ .... & .... & ... & .... \\ y_m(n) & y_m(n) & y_m(n) & y_m(n) \end{bmatrix} \tag{7}$$

y_i (j) = i = 1,2,..., m = SPIF experiment number, j = 1,2,..., n = output responses. In this case, n = 6, m = 18, and y = GRC of each output from Table 4. Equation (1) yields the correlation coefficient matrix C_{jl} (8),

$$C_{jl} = \left[\frac{\operatorname{cov}(y_i(j), y_i(l))}{\operatorname{sdev} y_i(j) \cdot \operatorname{sdev} y_i(l)}\right], j=1, 2,\ldots,n \text{ and } l=1,2\ldots,n, \tag{8}$$

where $\operatorname{cov}(y_i(j), y_i(l))$ is the covariance of orders of $y_i(j)$ and $y_i(l)$, $\operatorname{sdev} y_i(j)$ and $\sum_{k-1}^{n} \pi_k = n$ are the standard deviations of $y_i(j)$ and $y_i(l)$, respectively. The next step in PCA is to obtain the eigenvalues and eigenvectors from the matrix using Equation (9).

$$\left(C - \pi_k A_m\right) B_{ik} = 0 \tag{9}$$

A total of eighteen tests were performed, with one input parameter having two levels and the other four having three levels. Tables 6 and 7 show the eigenvalues and eigenvectors obtained using Equation (9). Table 8 shows the contribution of the initial principal component response. The square of the eigenvector matrix yields the value of the principal component contribution.

Table 3 S/N ratio for the obtained responses

Exp. no	S/N RATIO					
	Strain 1	Strain 2	Strain 3	Ra 1	Ra 2	Ra 3
1	-1.4497	-16.0621	-1.2667	-0.0950	-2.6969	-4.5734
2	-1.9277	-19.6568	-0.6921	-0.0213	-1.8340	-3.5192
3	-2.8365	-10.6119	-2.3198	-0.0864	-2.6906	-4.5657
4	-0.8354	-18.9442	-0.0048	-0.0039	-1.2824	-2.8324
5	-1.7288	-16.9186	-1.3113	-0.3490	-2.8859	-4.8012
6	-1.4702	-19.9047	-1.0744	-1.8333	-4.0176	-6.1459
7	-0.2589	-20.7064	-0.0763	-3.2453	-5.1348	-7.4437
8	-0.5486	-21.8777	-0.4140	-0.0424	-2.5298	-4.3710
9	-0.3646	-15.3155	-0.0500	-3.9841	-5.7341	-8.1293
10	-0.1079	-11.3912	-0.0186	-1.7917	-3.4669	-0.0213
11	-0.7297	-12.2079	-0.7094	-4.3660	-6.5535	-2.2789
12	-2.0386	-10.0049	-1.0597	-2.9170	-4.8386	-0.3906
13	-0.5065	-15.6145	-0.2423	-3.3705	-5.3811	-0.9921
14	-0.9520	-15.9591	-0.5415	-4.2229	-6.3865	-2.0966
15	-0.4790	-13.5933	-0.3630	-5.3673	-7.7105	-3.5334
16	-0.0212	-19.7663	-0.5757	-2.5686	-4.4181	-0.1089
17	-0.5158	-20.5656	-0.4759	-1.8551	-3.5452	-0.0028
18	-0.7655	-15.4265	-0.7948	-1.2449	-2.7853	-0.0677

Table 4 Normalised S/N ratio for the obtained responses

Exp. no	Normalised S/N RATIO					
	Strain 1	Strain 2	Strain 3	Ra 1	Ra 2	Ra 3
1	0.4926	0.4898	0.4549	0.9830	0.7799	0.4376
2	0.3228	0.1871	0.7031	0.9968	0.9142	0.5673
3	0.0000	0.9489	0.0000	0.9846	0.7809	0.4385
4	0.7108	0.2471	1.0000	1.0000	1.0000	0.6518
5	0.3935	0.4177	0.4356	0.9357	0.7506	0.4095
6	0.4853	0.1662	0.5380	0.6589	0.5745	0.2441
7	0.9156	0.0986	0.9691	0.3956	0.4007	0.0844
8	0.8127	0.0000	0.8232	0.9928	0.8060	0.4625
9	0.8780	0.5527	0.9805	0.2579	0.3075	0.0000
10	0.9692	0.8832	0.9940	0.6667	0.6602	0.9977
11	0.7483	0.8145	0.6956	0.1867	0.1800	0.7199
12	0.2834	1.0000	0.5443	0.4569	0.4468	0.9523
13	0.8276	0.5275	0.8974	0.3723	0.3624	0.8783
14	0.6694	0.4985	0.7682	0.2134	0.2060	0.7424
15	0.8374	0.6978	0.8453	0.0000	0.0000	0.5655
16	1.0000	0.1778	0.7534	0.5218	0.5122	0.9869
17	0.8243	0.1105	0.7965	0.6548	0.6480	1.0000
18	0.7356	0.5434	0.6588	0.7686	0.7662	0.9920

Table 5 Calculated grey relational coefficient (GRC) and grey relational grade (GRG) for 18 experiments

Exp. no	GRC						Weighted GRG	
	GRC Strain 1	GRC Strain 2	GRC Strain 3	GRC Ra 1	GRC Ra 2	GRC Ra 3	Grade	Rank
1	0.4963	0.4950	0.4784	0.9671	0.6944	0.4706	0.1121	11
2	0.4247	0.3808	0.6274	0.9936	0.8535	0.5361	0.2407	7
3	0.3333	0.9072	0.3333	0.9701	0.6954	0.4710	-0.3619	10
4	0.6335	0.3991	1.0000	1.0000	1.0000	0.5895	0.4861	2
5	0.4519	0.4620	0.4698	0.8860	0.6672	0.4585	0.1455	15
6	0.4928	0.3749	0.5197	0.5945	0.5403	0.3981	0.3759	18
7	0.8555	0.3568	0.9418	0.4528	0.4548	0.3532	0.7278	14
8	0.7275	0.3333	0.7388	0.9859	0.7204	0.4819	0.4357	6
9	0.8039	0.5278	0.9624	0.4025	0.4193	0.3333	0.5593	12
10	0.9420	0.8107	0.9882	0.6000	0.5954	0.9955	0.5000	1
11	0.6652	0.7293	0.6216	0.3807	0.3788	0.6410	0.3168	13
12	0.4110	1.0000	0.5232	0.4793	0.4747	0.9129	-0.0758	8
13	0.7436	0.5141	0.8298	0.4434	0.4395	0.8042	0.5807	9
14	0.6020	0.4993	0.6832	0.3886	0.3864	0.6599	0.4644	17
15	0.7546	0.6233	0.7637	0.3333	0.3333	0.5351	0.4687	16
16	1.0000	0.3782	0.6697	0.5112	0.5062	0.9745	0.9006	4
17	0.7400	0.3598	0.7107	0.5916	0.5868	1.0000	0.7126	5
18	0.6541	0.5227	0.5944	0.6836	0.6814	0.9843	0.4930	3

Table 6 shows that the first principal component (PC) has a considerable effect (42.6%); therefore, the percent contribution of the first PC was established as weighted production (Table 8). Thus, in Equation (6), the weighted coefficients were adjusted to μ_1 = 0.511, μ_2 = -0.559, μ_3 = 0.026, μ_4 = -0.477, μ_5 = 0.381, and μ_6 = 0.23. Table 5 shows the GRC and the weighted GRG for each combination performed after the substitution of the individual weight values.

Table 6 Eigen values and variations of principal components (PCs)

PC	Eigen value	Explained Variation (%)
First	2.558	42.6
Second	1.6454	27.4
Third	1.0509	17.5
Fourth	0.5549	9.2
Fifth	0.1711	2.8
Sixth	0.0199	0.33

The single GRG now optimizes the multi-objective optimization. Table 9 shows the average weighted GRG for each level. The higher the GRG number, the more influential the process parameter becomes. Accordingly, the optimal sequence of input process parameters was chosen as follows: tool diameter (A2 - 10 mm), wall angle (B3 – 66^o), step depth (C1 - 0.2 mm), spindle speed (D1 - 100 rpm), and feed rate (E2 - 1000 mm/min).

The ANOVA has a wide range of applications but it has been adopted in a minimum number of studies [28]. ANOVA assigns proportions to multiple inputs based on the variability of the response variable. It is possible to find the most important response variable. Fisher's F-test was used to determine the most critical forming parameter based on GRG. The results of the ANOVA for the weighted GRG are shown in Table 10.

The table shows that the wall angle contributes 52.44 percent, followed by step depth (18.55 percent), tool diameter (9.72 percent), spindle speed (1.64 percent), and feed rate (0.83 percent). Table 10 also shows that the range value of weighted GRG is the greatest for component B, then for C, A, D, and E in descending order. As it can be observed, wall angle (B) has a greater impact on the multi-objective response than other characteristics.

Table 7 Eigenvectors of PCs

Response variables	First	Second	Third	Fourth	Fifth	Sixth
Strain 1	0.511	0.362	0.151	-0.016	0.73	-0.227
Strain 2	-0.559	0.259	0.21	0.114	0.416	0.625
Strain 3	0.026	-0.631	0.259	0.689	0.23	-0.081
Ra 1	-0.477	0.378	0.381	0.188	-0.133	-0.657
Ra 2	0.381	0.493	0.052	0.592	-0.419	0.29
Ra 3	0.23	-0.135	0.847	-0.356	-0.219	0.188

Table 8 Contribution of response variables

Response variable	Contribution
Strain 1	4.5625
Strain 2	-4.9911
Strain 3	0.2321
Ra 1	-4.2589
Ra 2	3.4018
Ra 3	2.0536

Table 9 Response table for weighted GRG

Forming Parameter		Average weighted GRG				Rank
		Level 1	Level 2	Level 3	Range	
Tool diameter (mm)	A	0.3024	**0.4845#**		0.1821	3
Wall angle (°)	B	0.122	0.4202	**0.6382#**	0.5162	**1**
Step depth (mm)	C	**0.5512#**	0.386	0.2432	0.3080	2
Spindle speed (rpm)	D	**0.4426#**	0.352	0.3858	0.0906	4
Feed rate (mm/min)	E	0.415	**0.4904#**	0.356	0.0590	5
	Overall mean GRG = 0.3935, **# Optimum Level**					

Table 10 Results of ANOVA for weighted GRG

Source	DF	Sum of square	Mean square	F-value	F Critical α = 0.25	Contribution
A	1	0.14935	0.149346	4.62	1.5	9.72%
B	2	0.80579	0.402893	12.47	1.6	52.44%
C	2	0.28512	0.142558	4.41	1.6	18.55%
D	2	0.02515	0.012577	0.39	1.6	1.64%
E	2	0.01271	0.006356	0.2	1.6	0.83%
Error	8	0.2585	0.032312			16.82%
Total	17	1.53661				100.00%

As shown in Figure 3 (a) a tool diameter of 10 mm, a wall angle of 66°, a step depth of 0.2 mm, a spindle speed of 100 rpm, and a feed rate of 500 mm/min were found to be the optimum combination for achieving strain 1. Figure 3 (b) shows that the S/N ratio has the primary effect on strain 2. The maximum strain 2 was achieved with the following parameters: tool diameter of 10, step depth of 0.4, feed rate of 1500 mm/min, wall angle of 60°, and spindle

speed of 100 rpm. For strain 3, Figure 3 (c) shows the S/N ratio for primary effects. In order to achieve the maximum strain 3, the tool has to be 10 mm in diameter with a 0.2 step depth, 66° wall angle, 1000 mm/min feed rate, and 100 rpm spindle speed.

Figure 4 (a) shows the S/N ratio for the major impacts on Ra 1. A tool diameter of 10 mm, a spindle speed of 100 rpm, a wall angle of 63°, a step depth of 0.4 mm, and a feed rate of 500 mm/min were shown to be the best combination for achieving reduced Ra 1. Figure 4 (b) shows the S/N ratio for the major impacts on Ra 2. The ideal combination for achieving minimum Ra 2 was determined to be a tool diameter of 10 mm, a wall angle of 63°, a step depth of 0.4 mm, a spindle speed of 100 rpm, and a feed rate of 500 mm/min. Figure 4 (c) shows the S/N ratio for the major impacts on Ra 3. A tool diameter of 8 mm, a wall angle of 63°, a step depth of 0.4 mm, a spindle speed of 100 rpm, and a feed rate of 500 mm/min were shown to be the best combinations for achieving reduced Ra 3.

Confirmation tests check optimal parameter settings. The optimal predicted grey relational value is:

$$Y = Y_i + \sum \left(Y_n - Y_l \right) \tag{10}$$

where Y_i is the mean GRG, and Y_n is the mean GRG at optimal condition.

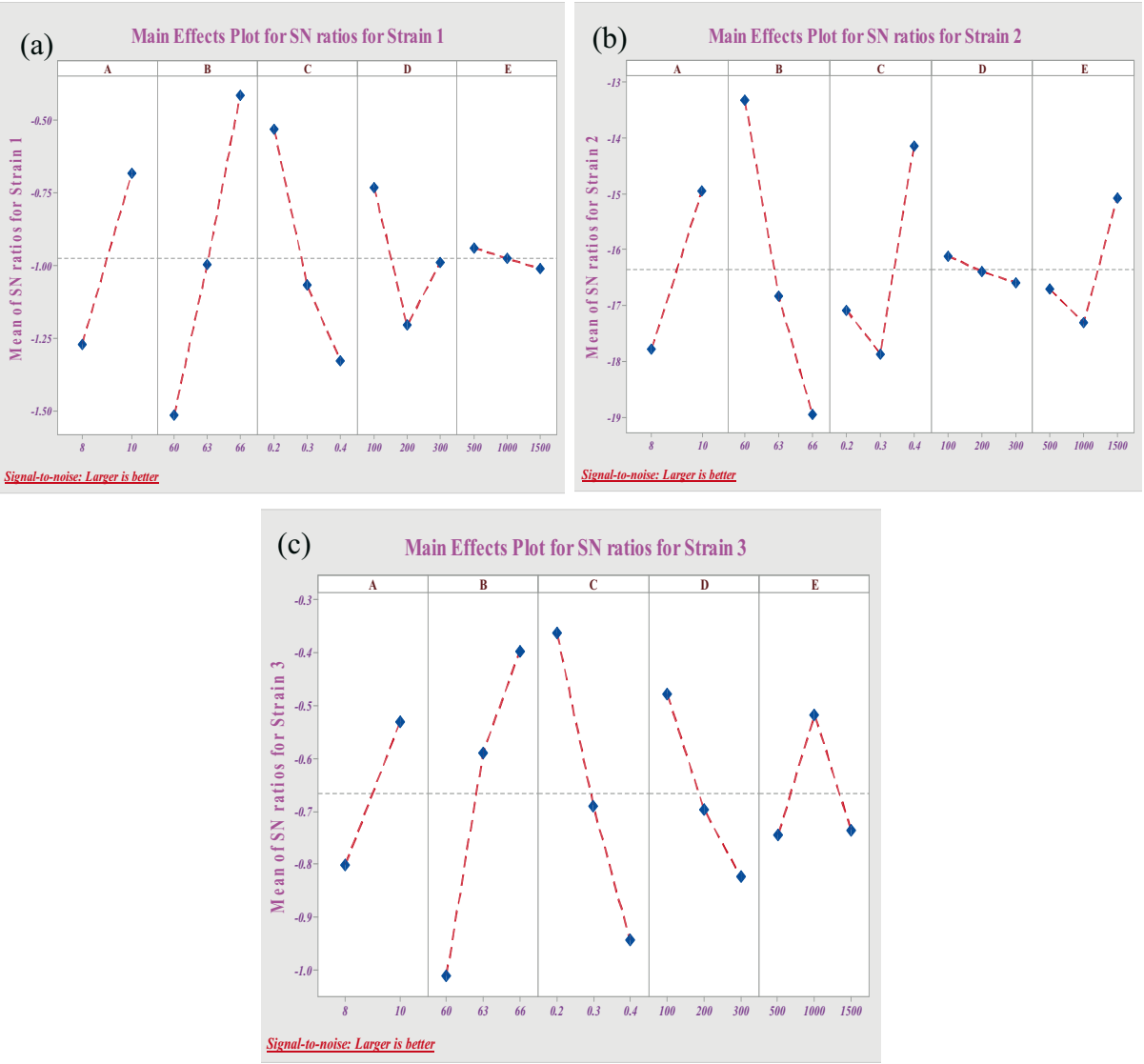

Fig. 3 **(a)** S/N ratio plot for Strain 1, **(b)** S/N ratio plot for Strain 2, **(c)** S/N ratio plot for Strain 3

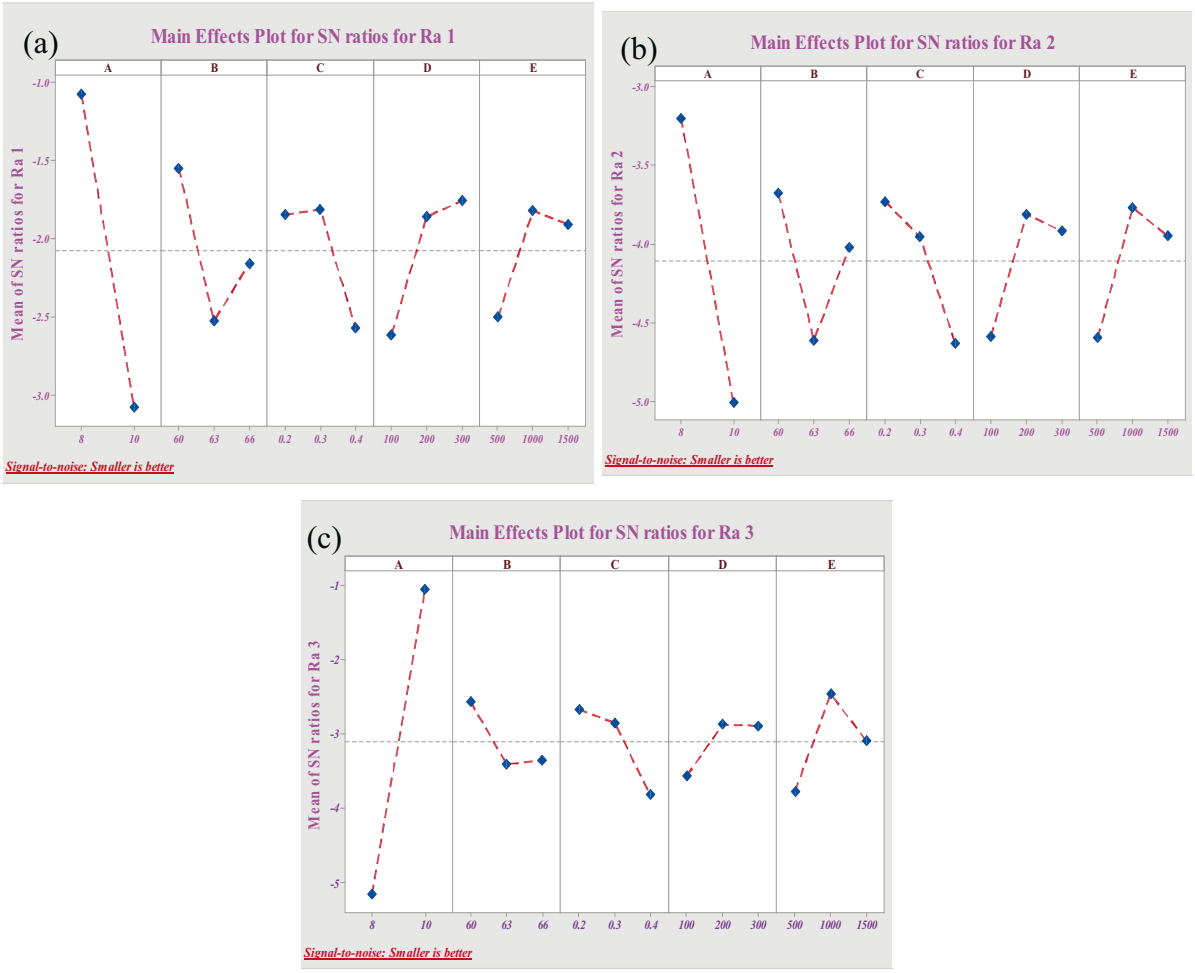

Fig. 4 **(a)** S/N ratio plot for Ra 1, **(b)** S/N ratio plot for Ra 2, **(c)** S/N ratio plot for Ra 3

Table 11 Results of confirmation experiments

Responses	Optimal parameter combination	
	Prediction	Experimental
	A2B3C1D1E2	A2B3C1D1E2
Strain 1	-	0.9936
Strain 2	-	0.3156
Strain 3	-	0.9992
Ra 1	-	1.1024
Ra 2	-	1.2687
Ra 3	-	1.0008
Weighted GRG	0.9575	0.9226

Table 11 shows the findings of the confirmation test, which revealed that the obtained GRG was 0.9226. The projected outcome was estimated at 0.9575. The GRG value obtained in the confirmation run was increased by 3.5 percent.

Figure 5 shows the structural modification of the component formed using the optimum process parameter combination. Location 1 depicts the unformed zone microstructure of the base metal. The SEM micrograph shows austenite grain boundaries and reveals unaltered austenite grains. Location 2 depicts the first developing zone, with marginal banding. The microstructure in cross-section shows the development of strain banding; austenite grains are undeformed but overlapped by bands. Location 4 demonstrates the severity of strain bands with

distorted austenite grains in the forming direction. Austenite grain fragmentation was detected. Location 5 has no banding owing to a minimal decrease in austenite grain fragmentation. However, the tension caused the development of slip bands.

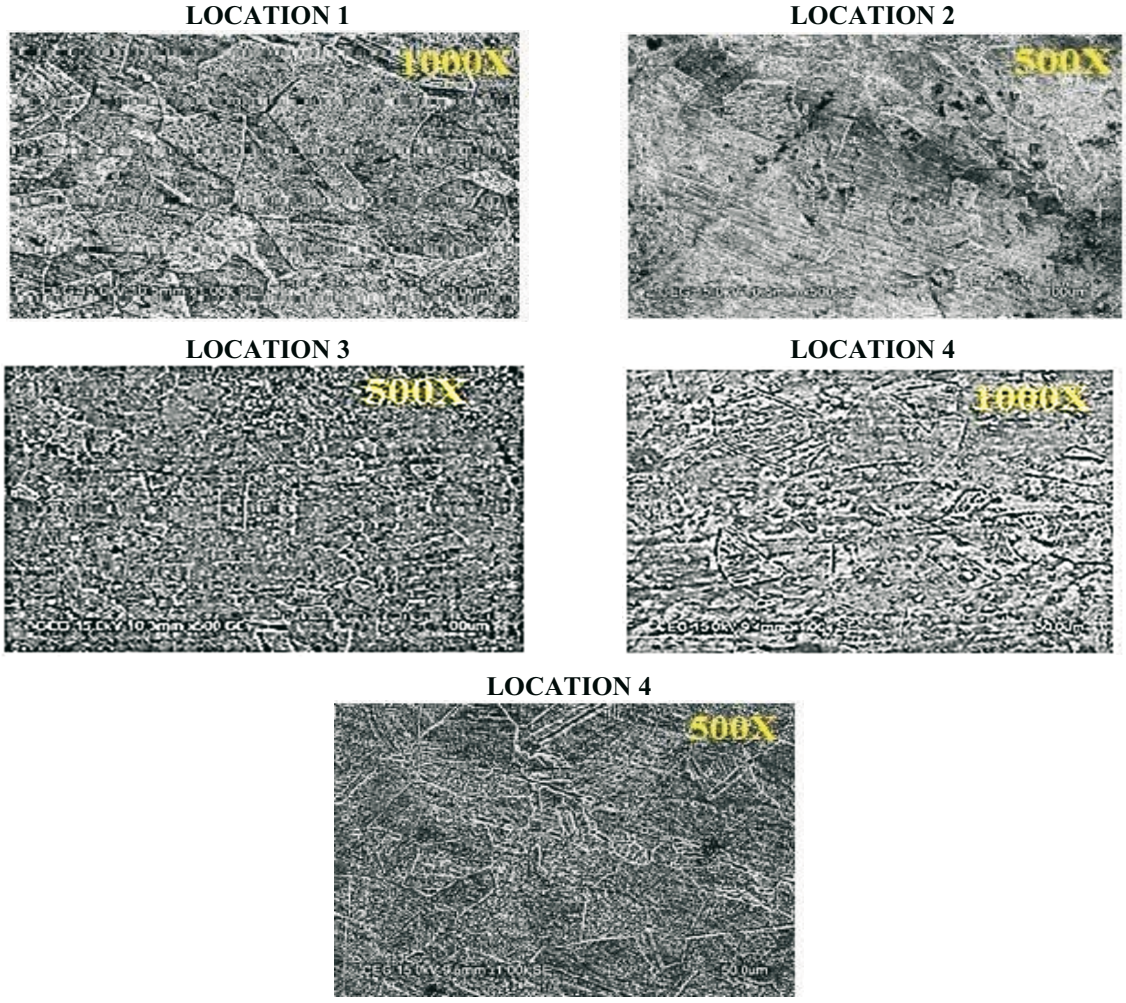

Fig. 5 SEM micrographs of the conformation specimen

4. Conclusion

A set of L_{18} experiments in the SPIF process using the grey relational analysis and the principal component analysis were done to assess the consistent weighting values of individual performance. A combination of GRA and PCA may efficiently find the optimum process parameters from validation studies. So, the following approach may be used to improve the SPIF process:

- From ANOVA results with a significance level of 95 %, it was concluded that the parameters that influence the strain and surface roughness are wall angle and step depth at 52.44 % and 18.55 %, respectively. Similarly, the parameters that have the least influence on the strain and surface roughness are tool diameter, spindle speed, and feed rate at 9.72 %, 1.64 %, and 0.83 %, respectively.
- The maximum strain and the minimum surface roughness can be obtained experimentally by keeping the parameters at the optimal combination of A2 (tool diameter of 10 mm), B3 (wall angle of 66º), C1 (step depth of 0.2 mm), D1 (spindle speed of 100 rpm), and E2 (feed rate of 1000 mm/min).

- The tool with a larger diameter will have a larger contact area with the sheet being formed, which increases formability.
- Lower surface roughness has been achieved while considering the higher end of the tool of 10 mm in diameter, a wall angle of 66^{o}, and a feed rate of 1500 mm/min. The higher strain has been achieved while considering a lower tool diameter of 8 mm, lower step depth of 0.2 mm, and a lower spindle speed of 100 rpm.
- The SEM micrograph shows grains of austenite not deformed during incremental forming.

REFERENCES

[1] Wisam K. H. Sarraji; Jamal Hussain;Wei-Xin Ren. Experimental Investigations on Forming Time in Negative Incremental Sheet Metal Forming Process: *Materials and Manufacturing Processes,* **2012**, 27, 499-506. https://doi.org/10.1080/10426914.2011.585550

[2] Hussain G; Khan H R; Gao L; Hayat H. Guidelines for Tool-Size Selection for Single-PointIncremental Forming of an Aerospace Alloy: *Materials and Manufacturing Processes,* **2013**, 28, 324-329. https://doi.org/10.1080/10426914.2012.700151

[3] Salah Echrif B M; Meftah Hrairi. Significant Parameters for the Surface Roughness inIncremental Forming Process: *Materials and Manufacturing Processes,* **2014**, 29, 697-703. https://doi.org/10.1080/10426914.2014.901519

[4] Raju C; Sathiya Narayanan C. Application of a hybrid optimization technique in a multiplesheet single point incremental forming process: *Measurement,* **2016**, 78, 296–308. https://doi.org/10.1016/j.measurement.2015.10.025

[5] Taleb Araghi B; Gottmann A; Bambach M; Hirt G; Bergweiler G; Diettrich J; Steiners M; Saeed-Akbari A. Review on the development of a hybrid incremental sheet forming system for small batch sizes and individualized production: *Production Engineering Research and Development,* **2011**, 5,393-404. https://doi.org/10.1007/s11740-011-0325-y

[6] Amrut Mulay; Satish Ben B; Syed Ismail; Andrzej Kocanda. Experimental Investigation and Modeling of Single Point Incremental Forming for AA5052-H32 Aluminum Alloy: *Arabian Journal of Science and Engineering,* **2017**, 42, 4929–4940. https://doi.org/10.1007/s13369-017-2746-1

[7] Lu H S; Chang C K; Hwang N C; Chung C T; Grey relational analysis coupled with principal component analysis for optimization design of the cutting parameters in high-speed end milling: *Journal of materials processing technology,* **2009**, 209, 3808–3817. https://doi.org/10.1016/j.jmatprotec.2008.08.030

[8] Pandivelan Chinnaiyan; Jeevanantham A K. Multi-Objective Optimization of Single Point Incremental Sheet Forming of AA5052 using Taguchi based Grey Relational Analysis Coupled with Principal Component Analysis: *International Journal of Precision Engineering and Manufacturing,* **2014**, 15(11), 2309-2316. https://doi.org/10.1007/s12541-014-0595-3

[9] Vishal Gulati; Ashmin Aryal; Puneet Katyal; Amitesh Goswami. Process Parameters Optimization in Single Point Incremental Forming: *Journal of the Institution of Engineers (India) Series C,* **2016**, 97(2), 185–193. https://doi.org/10.1007/s40032-015-0203-z

[10] Pratheesh Kumar S; Elangovan S. Optimization in single point incremental forming of Inconel 718 through response surface methodology: *Transactions of the Canadian Society for Mechanical Engineering,* **2020**, 44, 148-160. https://doi.org/10.1139/tcsme-2019-0003

[11] Suresh Kurra; Srinivasa Prakash Regalla; Rogelio Perez-Santiago. Study on the influence of process parameters in incremental forming using finite element simulations and Taguchi orthogonal array: *Advances in Materials and Processing Technologi*es, **2015**, 1(1-2), 201-209. https://doi.org/10.1080/2374068X.2015.1118993

[12] Ajay Kumar; Vishal Gulati. Experimental investigations and optimization of forming force in incremental sheet forming: *Sadhana,* **2018**, 43-159, 1-15. https://doi.org/10.1007/s12046-018-0926-7

[13] Ajay Kumar; Vishal Gulati. Experimental investigation and optimization of surface roughness in negative incremental forming: *Measuremen,t* **2019** , 131, 419–430. https://doi.org/10.1016/j.measurement.2018.08.078

[14] Angshuman Baruah;Pandivelan C; Jeevanantham A K. Optimization of AA5052 in incremental sheet forming using grey relational analysis: *Measurement,* **2017**, 106, 95–100. https://doi.org/10.1016/j.measurement.2017.04.029

[15] Mariem Dakhli; Atef Boulila; Pierre-Yves Manach; Zoubeir Tourki. Optimization of processing parameters and surface roughnessof metallic sheets plastically deformed by incremental forming process: *The International Journal of Advanced Manufacturing Technology,* **2019**, 102, 977-990. https://doi.org/10.1007/s00170-018-03265-x

[16] Seyed Ali Asghar Asghari; Asghar Shamsi Sarband; Mostafa Habibnia. Optimization of multiple quality characteristics in two-point incremental forming of aluminum 1050 by grey relational analysis: *Journal of Mechanical Engineering Science Part C,* **2017**, 1-15. https://doi.org/10.1177/0954406217693658

[17] Hani Mostafanezhad; Hossein Ghorbani Menghari; Samad Esmaeili; Ehsan Marzban Shirkharkolaee. Optimization of two-point incremental forming process of AA1050 through response surface methodology: *Measurement,* **2018**, 127, 21–28. https://doi.org/10.1016/j.measurement.2018.04.042

[18] Kuntal Maji ; Gautam Kumar. Inverse analysis and multi-objective optimization of Single-Point Incremental Forming of AA5083 aluminum alloy sheet: *Soft Computing,* **2020**, 24,4505-4521. https://doi.org/10.1007/s00500-019-04211-z

[19] Visagan A; Ganesh P. Influence of Higher Wall Angle on Formability in SPIF of AISI 316L: *Journal of Advanced Microscopy Research,* **2018**, 13, 1–5. https://doi.org/10.1166/jamr.2018.1388

[20] Ganesh P; Visagan A; Ethiraj N; Prabhahar M; Sendilvelan S. Optimization of pyramid shaped single point incremental forming of AA5052 alloy sheet: *Materials Today: Proceedings,* **2021**, 45, 5892–5898. https://doi.org/10.1016/j.matpr.2020.08.573

[21] Visagan A; Ganesh P. Parametric optimization of two point incremental forming using GRA and TOPSIS: *International Journal of Simulation Modeling, DAAAM International Vienna,* **2022**, 4, 615-626. https://doi.org/10.2507/IJSIMM21-4-622

[22] Visagan A; Ganesh P. Experimental Studies on Die based Two Point Incremental Forming: *International Journal of Vehicle Structures and system,* **2022**, 14(7), 912-917. https://doi.org/10.4273/ijvss.14.7.17

[23] Hongwei Gao; Qinhong Fan; Zhibing Chu. Simulation research on the forming process of large axis rolled by cross wedge rolling: *Transactions of FAMENA*, **2022**,46: 63-80. https://doi.org/10.21278/TOF.463043422

[24] Loganathan D; Satish Kumar S; Ramadoss R. Grey relational analysis-based optimization of input parameters of Incremental Forming process applied to the AA 6061 alloy: *Transactions of FAMENA*, **2020**, 44:93-104. https://doi.org/10.21278/TOF.44108

[25] Karthik K; Magudeeswaran G. Effects of gas metal arc welding variants on the mechanical nad microstructural characteristics of AISI 304 stainless steel: *Transactions of FAMENA*, **2023**,47:31-46. https://doi.org/10.21278/TOF.473048822

[26] Zhongfeng Zhang; Qingwen Xue; Lixia Wen; Weihua Peng; Han Shao; Wenzhi Fu. Study on Multi-step Forming Paths for Double Curved Parts of 1561 Aluminium Alloy: *Transactions of FAMENA*, **2023**, 47(2), 31-44. https://doi.org/10.21278/TOF.472051222

[27] Wafa Taktak ; Riadh Elleuch. Experimental Investigation Into the Effect of Cold Rolling on Fracture Toughness and Mechanical Properties of AA5754 H111 Aluminium Alloy: *Transactions of FAMENA*, **2023**, 47(2),67-78. https://doi.org/10.21278/TOF.472042322

[28] Nima Mirzaei. Solar collector performance analysis using ANOVA method: *Transactions of FAMENA*, **2021**, 45:29-41. https://doi.org/10.21278/TOF.454029621

Submitted: 02.6.2023

Accepted: 30.10.2023

A. Visagan*, Research Scholar
P. Ganesh, Associate Professor
Department of Production Technology, Anna University, Chennai, India
N. Ethiraj, Professor
Department of Mechanical Engineering, Dr.M.G.R Educational and Research Institute, Maduravoyal, Chennai, India
K. Kalaichelvan, Professor
Department of Ceramic Technology, Anna University, Chennai, India
*Corresponding author:
visaganarjunan69@gmail.com